JCI insight

ADAM17 variant causes hair loss via ubiquitin ligase TRIM47 mediated degradation

Xiaoxiao Wang, … , Hui Zhang, Ming Li

JCI Insight. 2024. https://doi.org/10.1172/jci.insight.177588.

Research In-Press Preview Dermatology Genetics

Graphical abstract

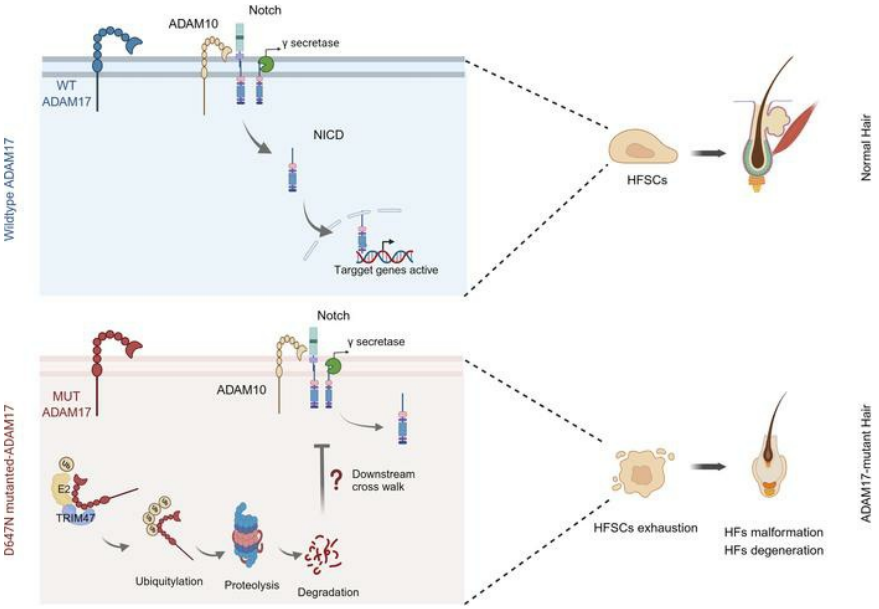

Find the latest version:

https://jci.me/177588/pdf

Title: *ADAM17* variant causes hair loss via ubiquitin ligase TRIM47 mediated degradation.

Author: Xiaoxiao Wang[1, 2, #], Chaolan Pan[1, 2, #], Luyao Zheng[1, 2, 3#], Jianbo Wang[4, #], Quan Zou[1, 2, #], Peiyi Sun[1, 2], Kaili Zhou[1, 2], Anqi Zhao[1, 5], Qiaoyu Cao[1, 5], Wei He[5], Yumeng Wang[1, 2], Ruhong Cheng[1, 2], Zhirong Yao[1, 2], Si Zhang[6, *], Hui Zhang[1, *], Ming Li[1, 5, *]

1. Department of Dermatology, Xinhua Hospital, Shanghai Jiaotong University School of Medicine, Shanghai 200092, China
2. Institute of Dermatology, Shanghai Jiaotong University School of Medicine, Shanghai 200092, China
3. Department of Dermatology, Anhui Provincial Children's Hospital, Hefei 230051, China.
4. Department of Dermatology, Henan Provincial People's Hospital, Zhengzhou University People's Hospital, Henan University People's Hospital, Zhengzhou 450003, China
5. Department of Dermatology, The Children's Hospital of Fudan University, Shanghai 201102, China.
6. NHC Key Laboratory of Glycoconjugate Research, Department of Biochemistry and Molecular Biology, School of Basic Medical Sciences, Fudan University, Shanghai 200032, China

[#] Authors contributed equally to this work.

***Correspondence:**

Address correspondence to: Ming Li, The Children's Hospital of Fudan University, 399 Wanyuan Road, Building 7#, Minhang District, Shanghai 201102, China; Phone: +86-21-64931226; Email: mingli@fudan.edu.cn;

Address correspondence to: Hui Zhang, Xinhua Hospital, Shanghai Jiaotong University School of Medicine, 1665 Kongjiang Road, Building 3#, Yangpu District, Shanghai 200092, China; Phone: +86-21-25076930; Email: zhanghui@xinhuamed.com.cn;

Address correspondence to: Si Zhang, School of Basic Medical Sciences, Fudan University, 137 Dong'an Road, Building West #7, Room 305, Xuhui District, Shanghai 200032, China; Phone: +86-21-54237223; Email: zhangsi@fudan.edu.cn.

Abstract

Hypotrichosis is a genetic disorder which characterized by a diffuse and progressive loss of scalp and/or body hair. Nonetheless, the causative genes for several affected individuals remain elusive, and the underlying mechanisms have yet to be fully elucidated. Here, we discovered a dominant variant in *ADAM17* gene caused hypotrichosis with woolly hair. *Adam17* (p.D647N) knock-in mice model mimicked the hair abnormality in patients. *ADAM17* (p.D647N) mutation led to hair follicle stem cells (HFSCs) exhaustion and caused abnormal hair follicles, ultimately resulting in alopecia. Mechanistic studies revealed that ADAM17 binds directly to E3 ubiquitin ligase TRIM47. *ADAM17* (p.D647N) variant enhanced the association between ADAM17 and TRIM47, leading to an increase in ubiquitination and subsequent degradation of ADAM17 protein. Furthermore, reduced ADAM17 protein expression affected Notch signaling pathway, impairing the activation, proliferation, and differentiation of HFSCs

during hair follicle regeneration. Overexpression of NICD rescued the reduced proliferation ability caused by *Adam17* variant in primary fibroblast cells.

Keywords: ADAM17, variant, hypotrichosis, TRIM47, HFSCs

Introduction

Human hair, especially human scalp hair, has important ornamental functions that are essential for social communication and senses of well-being. Unwanted hair loss poses psychosocial distress to affected individuals and impact on their quality of life (1). A comprehensive survey conducted on individuals suffering from hair loss revealed that they are more prone to experiencing anxiety, depression, and sleep disorders (2). Additionally, a concerning increase in suicide rates has been found among individuals suffering from hair loss (3, 4). Congenital hypotrichosis (HYPT) is a hair disorder marked by sparse or complete absence of hair on the scalp and/or other body parts. Occasionally, some cases accompanied by tightly coiled, curled, or woolly hair are called autosomal recessive woolly hair (ARWH) or autosomal dominant woolly hair (ADWH) depending on their congenital pattern (5, 6). *Keratin (KRT) 74* and *KRT71* mutations are known to cause non-syndromic ADWH1 (OMIM#613981) and ADWH2 (OMIM#615896), respectively (7, 8). Nevertheless, the causative genes for several affected individuals are still unidentified, and the underlying mechanisms have not been fully comprehended.

ADAM17, a type I transmembrane metallopeptidase, is responsible for shedding the ectodomains of over 90 substrates, including cytokines (such as TNFα), cytokine receptors (such as IL-6R and TNFR), and adhesion proteins (9). It functions as a

molecular switch to regulate both inflammation and tissue regeneration, and is linked to various inflammatory diseases, such as Alzheimer's disease, inflammation-related atherosclerosis, and rheumatoid arthritis (10-12). In addition, there is compelling evidence supporting the critical involvement of ADAM17 in many cancers and as potential therapeutic target (13-15). Even though ADAM17 can cleave multiple substrates *in vitro* or in cell-free assays, only some of them have a substantial impact on development and disease *in vivo*. For instance, in skin, deletion of ADAM17 in keratinocytes stimulates atopic dermatitis, driven by Th2 and/or Th17 response(s), due to a selective hindrance in the recruitment of the transcription factor c-Fos to the Th2-polarizing cytokine TSLP (16). ADAM17 regulates epidermal growth factor receptor (EGFR) ligand-dependent terminal keratinocyte differentiation, thus preserving the skin barrier (17). Additionally, ADAM17 is also involved in the development of the hair follicle inner root sheath (IRS) and the establishment of hair follicle stem cells (HFSCs) niche (18, 19). Despite receiving attention, further exploration is necessary to fully understand the impact of ADAM17 on hair follicle development.

Tripartite motif-containing protein 47 (TRIM47) functions as an E3 ubiquitin ligase and is involved in numerous biological processes, including tumorigenesis, cerebral ischemia-reperfusion injury and endothelial inflammation (20-24). The interaction between E3 ubiquitin ligase and the target protein is a core step in ubiquitin–proteasome system-mediated protein degradation (25). TRIM47 aggravates lipopolysaccharide-induced acute lung injury through the K63-linked ubiquitination of TRAF2 (26). TRIM47 promotes tumorigenesis by facilitating the ubiquitination and subsequent

degradation of SMAD4, FBP1, and PKC-ε/PKD3 (21, 23, 27). Nevertheless, the pathologic and clinical role of TRIM47 in hair follicles remain unclear.

In this study, we identified a variant in the CANDIS domain of *ADAM17* caused autosomal dominant hypotrichosis with woolly hair. *Adam17* knock-in mouse model mimicked the hair abnormality in patients. We discovered that TRIM47, an E3-ubiquitin ligase, interacted with the mutant ADAM17, promoting its ubiquitination and ultimate protein degradation. Eventually, reduced ADAM17 expression led to dysfunction in Notch signaling pathway, which in turn contributed to hair follicle malformation.

Results

ADAM17 variant leads to autosomal dominant hypotrichosis with woolly hair.

We conducted a study on a Chinese family consisting of seven patients afflicted with generalized hypotrichosis and curly hair. The majority of affected individuals exhibited tightly curled and sparse hair either at birth or during the early stage of infancy. The male patients exhibited varying degrees of hypotrichosis, often displaying fragile and thin scalp hair. Notably, they also had woolly hair, patchy hair loss of eyebrows, eyelashes, beard, moustache, axilla, and body. Hair growth tended to be limited, at a rate of 1-2cm since birth throughout their lifetime, leading to complete hair loss as they aged. Conversely, female patients presented milder symptoms in comparison to males, often showing only woolly hair and punctate or flaky alopecia (**Fig. 1A**). No abnormalities were detected concerning their skin, nails, teeth, or sweating.

Hematoxylin and eosin (HE) staining of scalp section exhibited a marked reduction in hair follicle counts, with minimal inflammatory infiltration observed around hair follicles (**Fig. 1B**). Scanning Electron Microscopy (SEM) imaging of healthy individuals' hair revealed a consistent ceramic tile-like arrangement of hair cuticles, whereas the patient displayed longitudinal grooves and cleavages. Moreover, the patient's hair exhibited irregular transverse sections and widespread exfoliation of the hair cuticle (**Fig. 1C**).

The provided pedigrees offered persuasive evidence supporting the autosomal dominant mode of inheritance for the phenotypes (**Fig. 1D**). To identify potential pathogenic variants associated with hypotrichosis causative genes like *KRT74, KRT25, KRT71, APCDD1, RPL21, SNRPE, CDSN, U2HR, EPS8L3, HR, DSG4, LIPH, LPAR6, DSC3, KRT25, LSS, TTMP, KRT86, KRT83,* and *KRT81* gene panel sequencing was used. However, the variant search yielded no results. We performed a genome-wide linkage analysis approach by single nucleotide polymorphisms (SNPs) and found evidence for linkage to chromosome 2 with a maximum LOD score of 3.18 (**Fig. 1E**). Subsequently, we narrowed down the candidate region to 19.6cM, between markers rs979290 and rs57254657, which encompassed 126 annotated genes, through genotyping of markers in the identified region (**Fig. S1**). We conducted the whole exome sequencing on an affected member (II: 4), screening all variants in the critical region, and detected a heterozygous missense mutation c.1939G>A (p. Asp647Asn) in the *ADAM17* gene (NM_003183). Upon conducting Sanger sequencing on all family members, we identified that the mutation was only detected in affected family members

(**Fig. 1F**). All identified variants were absent from public databases (Data ref: 1,000 genomes, ClinVar, Ensemble, and gnomAD) and 600 healthy controls.

Furthermore, ADAM17 is predominantly expressed in the hair cortex, IRS, and outer root sheath (ORS) of hair follicle (**Fig. 1G, Fig. S2**). Aspartic residue at position 647 is located within the conserved ADAM17 seventeen dynamic interaction sequence (CANDIS) domain of ADAM17, which is highly conserved and plays a vital role in protein interactions (**Fig. 1H-I**).

Adam17 (p.D647N) mutant mice model mimic hair loss in HYPT.

In order to ascertain whether the *ADAM17* (p.D647N) mutation is pathogenic, we constructed *Adam17* (p.D647N) knock-in mouse model using CRISPR/Cas9-mediated genome engineering (**Fig. S3A-B**). Homozygous mice ($Adam17^{D647N/D647N}$) were distinguishable from wild-type (WT) or heterozygous littermates ($Adam17^{D647N/+}$) due to their abnormal hair characteristics, including wavy vibrissa hair and a thinner, wavy and gray coat (**Fig. 2A**). These distinctive features first appeared shortly after birth and gradually worsened as the mice aged (**Fig. 2A**). Four hair follicle types with varying shapes and sizes emerged during hair development in the dorsal skin of mice, which including Guard (primary hair), Auchene and Awl (secondary hair) and Zigzag (tertiary hair) hairs (28). Compared with the wild-type, $Adam17^{D647N/D647N}$ pelages exhibited a reduction in primary and secondary hairs but a significant increase in the proportion of zigzag hairs. All four hair types in the $Adam17^{D647N/D647N}$ pelage displayed waviness, disorganized medulla, and irregular melanin piles (**Fig. 2B**). Furthermore, scanning electron microscopy reveals irregular and broken scales, suggesting a defect in the hair

cuticle (**Fig. 2C**).

HE staining showed that Adam17$^{D647N/D647N}$ mice exhibited a diminished count of hair follicles and abnormal hair architecture at the first anagen (Postnatal, P7) and the second anagen (P28) (**Fig. 2D-E**). Hair follicles in wild-type mice exhibited distinctive concentric layers, namely ORS, companion layer, IRS (Henle's layer, Huxley's layer, and cuticle) and hair shaft (cuticle, cortex, and medulla). However, the concentric structure of hair follicles in Adam17$^{D647N/D647N}$ mice was disrupted, along with a disturbed distribution of cells in the IRS (**Fig. 2D**). Additionally, hair shafts in the Adam17$^{D647N/D647N}$ mice displayed irregularities and deformities, suggesting a potential role for ADAM17 in hair shaft development (**Fig. 2E**). Immunofluorescence demonstrated that IRS labeled by Gata3 and hair cortex keratins labeled by the AE13 antibody, were markedly diminished in the hair follicles of Adam17$^{D647N/D647N}$ mice. Conversely, there was a noticeable increased expression of K5, which functioned as a pivotal marker for ORS (**Fig. 2F**). Furthermore, the Ki67 immunostaining revealed a decreased cell proliferation ability in hair germ of Adam17$^{D647N/D647N}$ mice (**Fig. 2F**). These observations were strengthened through western blotting (**Fig. 2G-H, Fig. S3C**). In addition, Transmission Electron Microscopy (TEM) demonstrated that hair follicles in wild-type mice exhibited distinctive concentric layers, while all layers apart from the hair shaft and IRS cuticle of hair follicles in Adam17$^{D647N/D647N}$ mice were indistinguishable (**Fig. 2I**). Overall, these results suggested that the p.D647N mutation in *ADAM17* had a substantial impact on the proper organization of hair follicles.

During the weaning period, Adam17$^{D647N/D647N}$ mice exhibited a distinguishable

shiny, red, and semi-transparent skin phenotype. Subsequently, at P15, a notable incidence of erythroderma developed along with a substantial amount of desquamation (**Fig. S3D**). Ultimately, this affliction resolved spontaneously in the subsequent days. Additionally, Adam17$^{D647N/D647N}$ mice experienced notable developmental retardation within the first four months (**Fig. S3E**). Remarkably, these mice displayed edema in their extremities and a significantly high mortality rate during the peri-weaning period (**Fig. S3F**). Conversely, no discernible anomalies were detected in the fur or skin of Adam17$^{D647N/+}$ mice as per our observation (**Fig. 2, Fig. S3**).

Disruption of HFSCs in *Adam17* (p.D647N) mutant mice contributes to the woolly hair and alopecia phenotype.

To further explore whether HFs in Adam17$^{D647N/D647N}$ mice are defected in forming new hair, we shaved hair and monitored the appearance of skin pigmentation. Adam17$^{D647N/D647N}$ mice exhibited a delayed onset of anagen in partial area of dorsal skin compared to their wild-type counterparts (**Fig. 3A-B**). This observation suggested that the *Adam17* (p.D647N) mutation hindered hair regeneration. HFs generate a new bulge besides the old one and persist to the next cycle in telogen periods, which called club hair (29). HE staining demonstrated a remarkably decrease of two-bulge HFs in telogen (P63) (**Fig. 3C, 3D left panel**). CD34 and K15 are specifically expressed in the inner and outer layers of the club hair, respectively, and are commonly used to label hair follicle stem cells (30). The whole-mount immunostaining against CD34 and K15 revealed that wild-type HFs developed a two-bulge architecture, whereas Adam17$^{D647N/D647N}$ mice usually had only one (**Fig. 3D right panel, 3E-F**).

198 At telogen, both wild-type and mutant bulge cells consisted of a α6 integrin (ITGA6)-
199 rich basal layer and an ITGA6-low suprabasal layer, both of which were CD34-positive.
200 Adam17$^{D647N/D647N}$ follicles displayed fewer CD34 positive bulge cells by fluorescence-
201 activated cell sorting (FACS) than wild-type follicles (**Fig. 3G upper panel**).
202 Adam17$^{D647N/D647N}$ follicles displayed lower Ki67 positive than wild-type follicles (**Fig.**
203 **3G lower panel**). Immunofluorescence of CD200, the marker of secondary hair germ
204 (SHG), confirmed a decreased differentiation of HFSCs in Adam17$^{D647N/D647N}$ mice at
205 early stage of anagen (P21) (**Fig. 3H**). Taken together, we find that the *Adam17*
206 (p.D647N) mutation leads to HFSCs abnormalities.

207 ***ADAM17*** **(p.D647N) mutation decreases its protein stability owing to the enhanced**
208 **auto-ubiquitination.**

209 To elucidate the potential impact of the p.D647N mutation on ADAM17, we
210 analyzed its expression in human subjects and mice samples. Notably, our
211 investigations revealed a significant reduction of ADAM17 protein levels in affected
212 individuals compared to healthy controls (**Fig. 4A-B**), although we did not observe any
213 significant differences in *ADAM17* mRNA levels (**Fig. 4C**). Correspondingly, we
214 observed a decrease in the protein level of Adam17, instead of mRNA levels, in hair
215 follicles of Adam17$^{D647N/D647N}$ mice (**Fig. 4D-F**). We postulated that this might be
216 attributable to the differential stability of two proteins, as mRNA levels could not
217 account for the difference in protein levels. To investigate the stabilities of two proteins,
218 we stably overexpressed wild-type and mutant ADAM17 in HaCaT cells, an
219 immortalized human keratinocyte line. Cycloheximide chase assays results indicated

that the mutant ADAM17 displayed a shorter half-life compared to the wild-type counterpart (**Fig. 4G, Fig. S4A**). Subsequently, we treated HaCaT cells with the proteasome inhibitor MG132 or lysosome inhibitor chloroquine (CQ). Our findings revealed that MG132, but not CQ, deterred the reduction of the mutant ADAM17 protein level relative to the wild-type counterpart, suggesting that the ubiquitin-proteasome pathway was involved in the further degradation of the mutant ADAM17 expression (**Fig. 4H-I, Fig. S4C and Fig.S4E**). Additionally, we verified that *Adam17* (p.D647N) mutation decreases its protein stability via ubiquitin-proteasome pathway in primary cultured fibroblasts from wildtype and Adam17$^{D647N/D647N}$ mice **(Fig. S4B, S4D and S4F)**. Indeed, hyper-ubiquitination of mutant ADAM17 was observed in HEK293T cells (**Fig. 4J**). In summary, our findings indicate that the mutant ADAM17 displays elevated auto-ubiquitination levels, ultimately leading to decreased protein stability and lower abundance.

Furthermore, we evaluated the shedding activity of ADAM17 in human skin tissue, as well as in primary cultured mouse skin fibroblast cells and HaCaT cells. Our findings indicated a significant reduction in ADAM17 shedding activity in the skin tissue of patients and primary cultured mouse skin fibroblast cells (**Fig S5A-B**). This reduction may be attributed to a decrease in the expression of ADAM17 (**Fig. 4A-C, Fig S4B**). It is worth noting that we overexpressed wild-type and mutant ADAM17 in HaCaT cells and observed no significant difference in shedding activity between the two groups at identical ADAM17 expression levels (**Fig S5C**). These results suggest that *ADAM17* variant does not impact its shedding activity.

ADAM17 (p.D647N) mutation reinforces the bond between ADAM17 and its specific E3 ubiquitin ligase, TRIM47

E3 ubiquitin ligases exhibit substrate specificity by selectively binding to target proteins, which results in their ubiquitination and subsequent degradation. To gain insight into the molecular mechanisms underlying *ADAM17* (p.D647N) mutation causes reduced protein stability, we set out to identify its E3 ubiquitin ligase by co-immunoprecipitation (co-IP) coupled with mass spectrometry. Through in-depth bioinformatic analysis of potential ADAM17-binding proteins identified, we located RING-E3 ligases TRIM47 as potential interactors of ADAM17 (**Fig. 5A-B, Table S1**). We validated the direct interaction between ADAM17 and TRIM47 using co-IP and pull-down assay (**Fig. 5C-D**). The endogenous association between Adam17 and Trim47 was then confirmed by co-immunoprecipitation assay in the epidermal tissue lysates of mice (**Fig. 5E**). Confocal immunofluorescence revealed that ADAM17 and TRIM47 were co-localized in HaCaT cells, primary cultured mouse skin fibroblasts, and hair follicles of mice (**Fig. 5F-H**). Moreover, Trim47 showed high expression in hair follicle stem cells (**Fig. S6A**). *ADAM17* (p.D647N) mutation strengthened the association between ADAM17 and TRIM47, confirming the mass spectrometry results (**Fig. 5B-G**). Subsequent to the aforementioned validation of direct interaction between ADAM17 and TRIM47, we probed the effect of knockdown/overexpression of TRIM47 in mutant ADAM17 HaCaT cells (**Fig. S6B**). Our results indicated that knockdown of TRIM47 impaired the degradation of the mutant ADAM17 (**Fig. 5I**), while overexpression of TRIM47 accentuated degradation of the mutant ADAM17 (**Fig.**

S6C). These results indicate that *ADAM17* (p.D647N) mutation reinforces the bond between ADAM17 and TRIM47, ultimately resulting in a reduced protein stability.

A computational 3D complex structural model by ZDock based on the X-ray crystal structure from the Protein Data Bank was further generated (**Fig. 5J, left panel**). Docking simulation data from the model demonstrated that amino acids D597, K626, D636, K640, D647, D657, L659, N671, and I672 of ADAM17 form a "hairpin" structure (**Fig. 5J, right upper panel**), and that amino acids F409, K425, Y428, D431, A476, R581, and R582 of TRIM47 form a "hairpin" structure (**Fig. 5J, right lower panel**). Based on the 3D complex structure model, it was deduced that these hairpin-like structures were accountable for facilitating their interaction.

ADAM17 deficiency blocks Notch signaling pathway consequently impaired hair follicle development.

To explore intrinsic effects resulting from the loss of ADAM17 expression, we performed proteomic analysis on the dorsal skin during the anagen phase (P28). Analysis of differentially expressed proteins (DEPs) revealed that *Adam17* variant led to broad changes in protein levels **(Fig. 6A-B)**. Specifically, we detected significant increase in ubiquinone and other terpenoid-quinone biosynthesis (Vkorc1, Coq6, and Coq3), along with the up-regulation of the Adam17-specific E3 ubiquitin ligase Trim47 (**Fig. 6A-B, Fig. S6D**). Then we confirmed the up-regulation of TRIM47 in mice skin samples and HaCaT cells (**Fig. S6E-G**). Our study revealed that *Adam17* (p.D647N) mutation markedly affect the proper development and organization of hair follicles. Indeed, significant reductions were observed in proteins related to keratinocyte

differentiation, hair follicle morphogenesis (**Fig. 6B**), especially proteins linked to hair shaft and IRS structure (**Fig. 6C**). Furthermore, KEGG pathway enrichment analysis demonstrated decreased activity within structural homeostasis-related pathways, including Notch signaling pathway, and cell adhesion pathway (**Fig. 6D**).

Previous research has indicated that ADAM17 can shed TGFα, which in turn actives EGFR signaling in hair follicles (18, 19). Thus, we conducted immunohistochemical staining to examine the influence of *Adam17* variant on the EGFR signaling pathway. Our findings revealed that the *Adam17* variant did not impact the expression of EGFR, as well as the phosphorylation of EGFR at Tyrosine 992 (p-EGFR (Try992)) and Tyrosine 1068 (p-EGFR (Try1068)) in $Adam17^{D647N/D647N}$ mice **(Fig. S7)**. Given that Notch signaling exerts regulatory effects on the differentiation of HFSCs into specific hair follicle cell types, is it plausible that Notch is the underlying cause of the hair loss phenotype observed in ADAM17 mutant mice? The activity of key molecules in the Notch signaling pathway were investigated in human subjects and mice samples. Ligand-mediated activation induces proteolytic cleavages of Notch and releases the NICD, which enters the nucleus and stimulates transcription of target genes (31). Our findings indicate a significant decrease in the protein level of NICD upon *ADAM17* (p.D647) variant, leading to decreased expression of Notch target genes, including *Hes1*, *Hes5*, *Hey1,* and *Hey2* (**Fig. 7A-B, Fig. S8A-B**). RT-PCR analysis demonstrated that the *Adam17* (p.D647N) mutation resulted in inhibited Notch target gene transcripts in mouse skin (**Fig. 7C**). Immunohistochemistry and immunofluorescence assays revealed a reduced amount of NICD in the hair follicles of mice during anagen (**Fig. 7D-E, Fig.**

S8C). The nuclear and cytoplasmic protein extraction assays further confirmed that the *ADAM17* (p.D647N) variants effectively inhibited the Notch signaling pathway in keratinocytes. This is supported by the observed reduction in the expression of NICD and its target genes within the cell nucleus **(Fig. 7F)**. To further investigate the involvement of the Notch signaling pathway in *Adam17* (p.D647N) mutation induced hair follicle malformation, we overexpressed NICD in primary cultured $Adam17^{D647N/D647N}$ mice skin fibroblasts. Our findings indicated that *Adam17* (p.D647N) mutation significantly reduced the proliferation ability of primary fibroblasts, which could be rescued by overexpression of NICD **(Fig. 7G-H, Fig. S8D-E)**. Collectively, our results confirm the relationship between the *ADAM17* (p.D647N) mutation and Notch activation in hair follicle development **(Fig. 7I)**.

Discussion

This study presented compelling evidence for the involvement of ADAM17 in the growth of hair follicles and differentiation of HFSCs, underscoring its significance as a potent molecule in the development of HYPT. Our investigation revealed that *ADAM17* (p.D647N) variant caused HYPT in human subjects, and *Adam17* (p.D647N) mutation mice model successfully emulated sparse and woolly hair observed in HYPT. Moreover, detailed mechanistic investigations demonstrated that *ADAM17* (p.D647N) mutation enhanced the interaction between ADAM17 and its E3 ubiquitin ligase TRIM47, leading to increased auto-ubiquitination and consequent degradation of ADAM17. Then reduced ADAM17 expression led to a decrease in the Notch signaling pathway, ultimately inhibiting the development of hair follicles.

Inherited hair loss disorders exhibit clinical and genetic heterogeneity, making it challenging to genotype patients accurately for diagnosis confirmation and genetic counseling. To date, over 14 detailed pathogenic genes of HYPT are reported to link with non-syndromic hypotrichosis, including hereditary hypotrichosis simplex (HHS), Marie Unna hereditary hypotrichosis (MUHH), localized autosomal recessive hypotrichosis (LAH), autosomal dominant woolly hair (ADWH) and autosomal recessive woolly hair (ARWH) (6-8, 32-37) (**Table S2**). HYPT3 and HYPT13 with pathogenic genes at *KRT74* and *KRT71* genes, respectively, were also classified as ADWH subtypes 1 and 2 (7, 8). In this study, we identified a novel subtype of congenital hypotrichosis with woolly hair that we designated ADWH3, caused by a heterozygous mutation in *ADAM17*. Affected females exhibited curly hair resembling steel wool, while males displayed a range of phenotypic severity from limited to complete baldness, notwithstanding the pervasive thinning of body hair. Unlike HHS and LAH, which only affects scalp hair or limits to some areas (36), ADWH3's phenotypes were distinguished by a general scarcity of hair throughout the body. Nonetheless, typical of other forms of HYPT, progressive hair loss with age was also extensive (38, 39). Given the challenges associated with distinguishing this type of disorder from other congenital HYPT, genetic testing assumes critical importance.

Although the dominant variant in the *ADAM17* gene causes hypotrichosis with woolly hair in humans, homozygous variants are necessary to observe the phenotype in mice. Notably, the homozygous mice, exhibiting a more severe phenotype than heterozygous patients, characterized by developmental retardation, edema in their

extremities, and a significantly high mortality rate during the peri-weaning period. This phenotypic difference is likely due to genetic and biological disparities between mice and humans (40). It is important to note the phenotypes observed in animal models may vary from those observed in humans (41). For instance, HPRT deficiency does not constitute a pathological variant in mice, despite its association with severe Lesch-Nyhan syndrome in human hemizygotes (42, 43). In our study, we found that the heterozygous variant in the *ADAM17* gene impaired stability and exhibited haplo-insufficiency in humans, while heterozygous variants maintained adequate protein levels, potentially averting hair development abnormalities in mice. However, further experimental investigation is necessary to fully understand the underlying mechanism.

ADAM17, a type I transmembrane protein, is composed of multiple domains. Mutations within these domains can lead to a range of disorders, indicating the sensitivity and delicacy of its structure and function. For instance, mutations in the pro-domain (PD) domain have been identified as a key driver of colorectal cancer (44) and late-onset Alzheimer's disease (10). Compound heterozygous mutations in the membrane proximal domain (MPD) and homozygous deletions in disintegrin domain (MD) result in neonatal inflammatory skin and bowel disease 1 (NISBD1, OMIM#614328) (45, 46). Notably, to date, there are no reported mutations in the highly conserved CANDIS domain. Here, we identified a heterozygous variant in the CANDIS domain of ADAM17 that caused non-syndromic ADWH3. Further mechanistic investigations revealed that the variant in CANDIS enhanced ADAM17 susceptibility to ubiquitin-mediated degradation by enhancing its association with E3 ubiquitin ligase

TRIM47. Ubiquitination is a critical posttranslational modification that plays a pivotal role in protein degradation via the proteasome (25, 47). Additionally, various posttranslational modifications play a crucial role in the rapid and reversible activation of ADAM17 (48-50). For instance, cytoplasmic phosphorylation of ADAM17 can regulate its activation, as well as rapid transport to the cell surface (51), which provides a mechanism for fine-tuning ADAM17 activity in response to cellular signals. Our studies enriched the understanding of the complex regulatory mechanisms that govern ADAM17 function and highlight the importance of structural conservation within the CANDIS domain.

Notch pathway is a highly conserved pathway, which exerts regulatory effects on the differentiation of HFSCs into specific hair follicle cell types and represses their differentiation towards the epidermal cell fate (52). Notch signaling also regulates the skin microbiome and inflammation of HFSCs niche, protecting the hair follicle from inflammatory damage (53). Notch1-deficient mice exhibited a thinner, shorter, and wavy appearance, accompanied by a defect in the hair cuticle (54), which were also observed in $Adam17^{D647N/D647N}$ mice. In addition, we identified a significant decrease in the expression of key molecules associated with the Notch signaling pathway in both patients and $Adam17^{D647N/D647N}$ mice. These finding establish a correlation between ADAM17 and Notch signaling, which has been previously reported in various diseases, including prostate tumors, non-small cell lung carcinoma, hepatocellular carcinoma and diabetic nephropathy (55-57).

However, the classical viewpoint suggests ADAM10 directly cleaves the S2 site of

Notch1 and produces NICD to take effects (53, 58-61), while ADAM17 can only activate Notch signaling in non-physiological conditions *in vitro* (62-66). ADAM10-Notch signaling axis mediated regulation of host-microbial symbiosis crucially protects HFs from inflammatory destruction. Disruption of this signaling axis leads to skin dysbiosis and hair follicle destruction mediated by innate lymphoid cells (53). However, a recent study illustrated that *FGFR2* variants resulted in the activation of EGFR and Notch signaling pathways, along with ADAM10, in an ADAM17-dependent manner (67). Although the molecular mechanisms underlying the crosstalk between ADAM17 and ADAM10 mediated Notch were unknown, it is possibly that aberrant activation of ADAM17/EGFR pathways reduces ADAM10 proteolytic activity or alternatively decreases its substrate accessibility (67). Moreover, ADAM17/EGFR signaling promotes the development of the IRS, which is crucial for hair shaft formation (18). However, our findings demonstrated that *Adam17* variant did not impact the expression or phosphorylation of EGFR in Adam17$^{D647N/D647N}$ mice. Based on these, we speculate that the downregulation of Notch signaling observed in our study appears to be a secondary effect resulting from dysfunction in the downstream signaling of ADAM17. Future studies are necessary to investigate whether other signaling pathways also contribute to *ADAM17* variant mediated hair malformations. Understanding the complex interactions between different signaling pathways and their role in hair follicle development may offer insights into potential therapeutic targets for hair loss and other related disorders.

Conclusions

Collectively, this study offers valuable insights into the post-translational modification of ADAM17, highlighting its pivotal function in hair follicle development and expanding the range of inherited hypotrichosis disorders. Our discoveries reveal new possibilities for therapeutic targets for hair loss.

Methods

Sex as a biological variable

To ensure the generalizability and relevance of our findings across genders, we included both male and female human participants, as well as male and female mice in our study. However, in the mice portion of the study, sex was not treated as a biological variable due to the absence of observed sex-specific differences in any of the measured endpoints between male and female mice.

Whole-exome sequencing analysis and pathogenic gene identification

Whole-exome sequencing analysis and pathogenic gene identification were performed using patient's blood as described previously (68). Comprehensive sequencing data analysis was performed based on autosomal dominant inheritance. Genome-wide linkage analysis was performed with a total of 5789 SNP markers; their average genetic and physical distance were 436 kb and 0.56 cM respectively. In the linkage analysis, we removed SNPs with a call rate less than 90% monomorphic SNPs, and non-Mendelian transmitted markers, and retained a total number of 4532 informative autosomal SNPs. Multipoint parametric linkage analyses were performed using the MERLIN program version 1.1.2. A fully penetrant autosomal-dominant model was used with a rare disease frequency of 0.0001. Critical recombination events of the

pedigree members were determined through haplotype construction in MERLIN.

Generation of *Adam17* (p.D647N) mutation mice

Adam17 (p.D647N) mutation mice were generated using CRISPR/Cas9-mediated genome engineering (Cyagen Biosciences (Suzhou), China). To introduce the desired mutation, a gRNA targeting the mouse *Adam17* gene, a donor oligo carrying the p.D647N (GAC to AAC) mutation, a synonymous mutation (p. R651= (CGA to AGG)), and Cas9 were co-injected into fertilized mouse eggs, resulting in targeted knock-in offspring. F0 founder animals were identified by PCR and subsequent sequence analysis. The founder animals were then bred to wild-type mice to assess germ line transmission and F1 animal generation. Heterozygous F1 mice were intercrossed to generate F2 mice. To identify Adam17 mutant mice, genomic tail DNA was isolated and subjected to routine genotyping by PCR and subsequent sequence analysis. The primers utilized for PCR and Sanger sequencing are provided in **Table S3**. All animals were group-housed under normal light-dark cycle with food and water ad libitum.

Cell culture

HaCaT cell lines were purchased from Chinese Academy of Sciences Shanghai Branch Cell Bank (China). Cells were cultured in Dulbecco's modified Eagle's medium (DMEM) (Gibco, USA), which was supplemented with 10% fetal bovine serum (Gibco, USA) and 1% penicillin-streptomycin (Gibco, USA).

Tyramide signal amplification (TSA) multiple immunofluorescence assay

TSA multiple immunofluorescences staining experiments were conducted following

the manufacturer's instructions (Shanghai Recordbio Technology, China). Paraffin-embedded skin sections were hydrated sequentially in xylene and gradient ethanol. Sections underwent antigen retrieval with a citrate repair buffer at pH 6.0, and blocked with 10% horse serum in PBS at room temperature for 1 h using 10% horse serum in PBS. Primary antibody was added to the sections and incubated overnight at 4°C. After that, horseradish peroxidase (HRP)-conjugated secondary antibodies were added and incubated at room temperature for 1 hour. Finally, the sections were incubated with indicated tyramide fluorescent dyes for 15 minutes at room temperature to complete the fluorescence staining of multiple antibodies. Repeat the above steps starting from the antigen retrieval step for the next primary antibody. The antibodies and their dilutions used in this study were listed in **Table S4**.

Flow cytometry

Skin epidermal cell suspensions were obtained from defined areas of back skin. Skin was minced and incubated overnight in Hank's Balanced Salt Solution buffer (Thermo Fisher Scientific, USA) containing 5 mg/ml Dispase II (Yeasen, China). Next day, the separated epidermal tissue was added to 0.05% trypsin (Thermo Fisher Scientific, USA) with 100 μg/mL DNase I (Sigma-Aldrich, USA) and agitated for 10 minutes. Thereafter, suspension cells were passed through a 75-μm sieve (Millipore, Germany), and sequentially stained with Fixable Viability Dye eFluor 455UV, anti-CD34 eFluor 660, and anti-ITGA6 PE, and anti-Ki67 FITC antibodies. Data were acquired using a BD LSRFortessa X-20 (BD, USA) instrument and analyzed on FlowJo software (FlowJo, USA).

Western blot

Total protein was extracted from cells and tissues by using RIPA lysis buffer, and then subjected to separation using sodium dodecyl sulfate-polyacrylamide gel electrophoresis (SDS-PAGE) and subsequently electro-transferred onto a polyvinylidene difluoride (PVDF) membrane (Millipore, Germany), in accordance with previously established protocols (69). Thereafter, the membrane was blocked with 3% BSA at room temperature for 60 minutes, and then incubated overnight with primary antibodies as indicated. Following this, the membrane was incubated with secondary antibodies for 1.5 hours. The details of the antibodies and their respective dilutions used in this study are provided in **Table S4**.

Quantitative real time PCR (RT-PCR)

Total RNA was extracted from mouse skin or cells using the RNeasy kit, following the manufacturer's instructions. The mRNA was reverse-transcribed into cDNA using the PrimeScript RT Reagent kit (Takara, Japan). Gene expression was quantified in real-time using the SYBR Premix Ex Taq kit (Takara, Japan) on a Quantstudio3 (Applied Biosystems, USA) according to the manufacturer's protocols. Primers used for RT-PCR are provided in **Table S3**. Relative expression was normalized for levels of β-actin.

***In vivo* ubiquitination assays**

HEK293T cells were transfected with His-tagged ubiquitin and indicated plasmids. After 24 hours, MG-132 (MCE, USA) was added for 8 h, followed by cell lysis in immunoprecipitation lysis buffer. The lysates were pre-cleared with protein A/G beads for 3 hours, and the cleared supernatants were incubated with HA-tagged antibodies

and protein A/G beads at 4 °C for 16 hours. Following this, the pull-down products were washed three times with IP lysis buffer and detected immunoblotting. The details of the antibodies and their respective dilutions used in this study are provided in **Table S2**.

Protein stability and degradation

Cycloheximide chase assays were performed on HaCaT cells seeded into 12-well plates to 80-90% confluency. The following day, cells were treated with 50 μM Cycloheximide (MCE, USA) for 2, 4, 6, 8, and 12 hours, respectively. The cells were then lysed with RIPA lysis buffer and analyzed by western blot.

Protein degradation by proteasomes pathway was investigated in HaCaT cells seeded in 12-well plates at 80-90% confluence. The next day, cells were treated with 10 μM MG132 (MCE, USA) for 2, 4, 6, 8, and 12 hours. The cells were then lysed with RIPA buffer and analyzed using Western blotting.

Protein degradation by autophagy pathway was investigated in HaCaT cells seeded in 12-well plates at 80-90% confluence. The next day, cells were treated with 50 μM Hydroxychloroquine (MCE, USA) for 2, 4, 6, 8, and 12 hours. The cells were then lysed with RIPA buffer and analyzed using Western blotting.

Pull-down assay

His-tagged TRIM47 proteins were expressed in bacterial BL21 cells. Following bacterial lysis, His-tagged TRIM47 was purified using Ni-NTA beads (Thermo Fisher Scientific, USA). To investigate the direct interaction between TRIM47 and ADAM17, purified TRIM47 was incubated with *in vitro*-translated wild-type or mutant ADAM17

overnight at 4 °C. After washing with ice-cold buffer, proteins were eluted from the beads and detected by immunoblotting.

Statistics

All data were analyzed statistically using GraphPad Prism Version 8.0 (La Jolla, USA). All results were presented as mean ± SD. Shapiro-Wilk test was performed to check the data distribution. Unpaired two-tailed t-tests or Mann Whitney two-tailed tests were utilized for comparisons between two groups. For comparison among multiple groups, ordinary one-way ANOVA with Dunnett's post hoc or Kruskal-Wallis test followed by Dunn's post hoc was used based on the Gaussian or non-Gaussian distribution of the data. $P < 0.05$ (two-side) was considered statistically significant.

Study approval

This study was approved by Xinhua Hospital, Shanghai Jiaotong University School of Medicine and was conducted in accordance with the Declaration of Helsinki and the Department of Health and Human Services Belmont Report. All animal experiments adhered to the regulations specified in the National Academy of Sciences Laboratory Animal Care and Use Guidelines. Approval for conducting animal studies was obtained from the Animal Studies Committee at Xinhua Hospital Affiliated to Shanghai Jiaotong University School of Medicine.

Data availability

The datasets supporting the conclusions of this article are included within the article and its additional files. All supporting data values pertinent to the main manuscript and supplementary materials, including numerical values for all data points depicted in

graphs and the underlying values for any reported means, were comprehensively included in the supporting data values file. In this study, the produced data sets are available in the following databases: The mass spectrometry proteomics data and protein interaction AP-MS data have been submitted to the ProteomeXchange Consortium (https://proteomecentral.proteomexchange.org) via the iProX partner repository, with the dataset identifiers PXD049458 and PXD049459, respectively. Human variations data have been submitted to CNGB Sequence Archive (CNSA) (https://db.cngb.org/cnsa/) with the dataset identifiers sub052490.

Author's contributions

XW and ML designed and conceived this project developed methodology. XW, CP, QZ, WH, KZ, YW, AZ, QC and FC performed experiments and generated data. JW, LZ and CW conducted collection of clinical patient data and relevant specimens. XW, PS, WC, HL and GL analyzed and interpreted data. XW and CP wrote the draft. ML, SZ, ZY and HZ revised and finalized the manuscript. All authors contributed to and approved the manuscript. The order of co-first authors is determined based on the contributions of each author.

Acknowledgments

This work was supported by grants from the National Natural Science Foundation of China (82073422, 82273504 and 82303990), Shanghai Municipal Natural Science Foundation (22YF1427100, 22ZR1440800, and 20ZR1434900), Medical Engineering Cross Research Foundation of Shanghai Jiaotong University (YG2022ZD010, YG2022QN040) and Clinical Research Plan of SHDC (SHDC22022302). We greatly

appreciate the patients and their relatives for their participation in this study. We thank the Core Facility of Basic Medical Sciences, Shanghai Jiaotong University School of Medicine for LC–MS/MS and Transmission electron microscopy analyzing.

Conflict of interest

The authors have declared that no conflict of interest exists.

References

1. Chen CL, Huang WY, Wang EHC, Tai KY, and Lin SJ. Functional complexity of hair follicle stem cell niche and therapeutic targeting of niche dysfunction for hair regeneration. *Journal of biomedical science.* 2020;27(1):43.
2. Singam V, Patel KR, Lee HH, Rastogi S, and Silverberg JI. Association of alopecia areata with hospitalization for mental health disorders in US adults. *Journal of the American Academy of Dermatology.* 2019;80(3):792-4.
3. Prendke M, Kanti-Schmidt V, Wilborn D, Hillmann K, Singh R, Vogt A, et al. Quality of life in children and adolescents with alopecia areata-A systematic review. *Journal of the European Academy of Dermatology and Venereology : JEADV.* 2023.
4. Toussi A, Barton VR, Le ST, Agbai ON, and Kiuru M. Psychosocial and psychiatric comorbidities and health-related quality of life in alopecia areata: A systematic review. *Journal of the American Academy of Dermatology.* 2021;85(1):162-75.
5. Wasif N, Naqvi SK, Basit S, Ali N, Ansar M, and Ahmad W. Novel mutations in the keratin-74 (KRT74) gene underlie autosomal dominant woolly hair/hypotrichosis in Pakistani families. *Human genetics.* 2011;129(4):419-24.
6. Wen Y, Liu Y, Xu Y, Zhao Y, Hua R, Wang K, et al. Loss-of-function mutations of an inhibitory upstream ORF in the human hairless transcript cause Marie Unna hereditary hypotrichosis. *Nature genetics.* 2009;41(2):228-33.
7. Shimomura Y, Wajid M, Petukhova L, Kurban M, and Christiano AM. Autosomal-dominant woolly hair resulting from disruption of keratin 74 (KRT74), a potential determinant of human hair texture. *American journal of human genetics.* 2010;86(4):632-8.
8. Fujimoto A, Farooq M, Fujikawa H, Inoue A, Ohyama M, Ehama R, et al. A missense mutation within the helix initiation motif of the keratin K71 gene underlies autosomal dominant woolly hair/hypotrichosis. *The Journal of investigative dermatology.* 2012;132(10):2342-9.
9. Scheller J, Chalaris A, Garbers C, and Rose-John S. ADAM17: a molecular switch to control inflammation and tissue regeneration. *Trends in immunology.* 2011;32(8):380-7.

10. Hartl D, May P, Gu W, Mayhaus M, Pichler S, Spaniol C, et al. A rare loss-of-function variant of ADAM17 is associated with late-onset familial Alzheimer disease. *Molecular psychiatry.* 2020;25(3):629-39.
11. Tang BY, Ge J, Wu Y, Wen J, and Tang XH. The Role of ADAM17 in Inflammation-Related Atherosclerosis. *Journal of cardiovascular translational research.* 2022;15(6):1283-96.
12. Song Y, Jo S, Chung JY, Oh Y, Yoon S, Lee YL, et al. RNA interference-mediated suppression of TNF-α converting enzyme as an alternative anti-TNF-α therapy for rheumatoid arthritis. *Journal of controlled release : official journal of the Controlled Release Society.* 2021;330:1300-12.
13. Gao MQ, Kim BG, Kang S, Choi YP, Yoon JH, and Cho NH. Human breast cancer-associated fibroblasts enhance cancer cell proliferation through increased TGF-α cleavage by ADAM17. *Cancer letters.* 2013;336(1):240-6.
14. Pelullo M, Nardozza F, Zema S, Quaranta R, Nicoletti C, Besharat ZM, et al. Kras/ADAM17-Dependent Jag1-ICD Reverse Signaling Sustains Colorectal Cancer Progression and Chemoresistance. *Cancer research.* 2019;79(21):5575-86.
15. Bolik J, Krause F, Stevanovic M, Gandraß M, Thomsen I, Schacht SS, et al. Inhibition of ADAM17 impairs endothelial cell necroptosis and blocks metastasis. *The Journal of experimental medicine.* 2022;219(1):e20201039.
16. Murthy A, Shao YW, Narala SR, Molyneux SD, Zúñiga-Pflücker JC, and Khokha R. Notch activation by the metalloproteinase ADAM17 regulates myeloproliferation and atopic barrier immunity by suppressing epithelial cytokine synthesis. *Immunity.* 2012;36(1):105-19.
17. Franzke CW, Cobzaru C, Triantafyllopoulou A, Löffek S, Horiuchi K, Threadgill DW, et al. Epidermal ADAM17 maintains the skin barrier by regulating EGFR ligand-dependent terminal keratinocyte differentiation. *The Journal of experimental medicine.* 2012;209(6):1105-19.
18. Inoue A, Arima N, Ishiguro J, Prestwich GD, Arai H, and Aoki J. LPA-producing enzyme PA-PLA$_1$α regulates hair follicle development by modulating EGFR signalling. *The EMBO journal.* 2011;30(20):4248-60.
19. Nagao K, Kobayashi T, Ohyama M, Akiyama H, Horiuchi K, and Amagai M. Brief report: requirement of TACE/ADAM17 for hair follicle bulge niche establishment. *Stem cells (Dayton, Ohio).* 2012;30(8):1781-5.
20. Dou S, Li G, Li G, Hou C, Zheng Y, Tang L, et al. Ubiquitination and degradation of NF90 by Tim-3 inhibits antiviral innate immunity. *eLife.* 2021;10:e66501.
21. Liang Q, Tang C, Tang M, Zhang Q, Gao Y, and Ge Z. TRIM47 is up-regulated in colorectal cancer, promoting ubiquitination and degradation of SMAD4. *Journal of experimental & clinical cancer research : CR.* 2019;38(1):159.
22. Ji YX, Huang Z, Yang X, Wang X, Zhao LP, Wang PX, et al. The deubiquitinating enzyme cylindromatosis mitigates nonalcoholic steatohepatitis. *Nature medicine.* 2018;24(2):213-23.
23. Li L, Yu Y, Zhang Z, Guo Y, Yin T, Wu H, et al. TRIM47 accelerates aerobic

glycolysis and tumor progression through regulating ubiquitination of FBP1 in pancreatic cancer. *Pharmacological research.* 2021;166:105429.
24. Chen JX, Xu D, Cao JW, Zuo L, Han ZT, Tian YJ, et al. TRIM47 promotes malignant progression of renal cell carcinoma by degrading P53 through ubiquitination. *Cancer cell international.* 2021;21(1):129.
25. Morreale FE, and Walden H. Types of Ubiquitin Ligases. *Cell.* 2016;165(1):248-.e1.
26. Qian Y, Wang Z, Lin H, Lei T, Zhou Z, Huang W, et al. TRIM47 is a novel endothelial activation factor that aggravates lipopolysaccharide-induced acute lung injury in mice via K63-linked ubiquitination of TRAF2. *Signal transduction and targeted therapy.* 2022;7(1):148.
27. Azuma K, Ikeda K, Suzuki T, Aogi K, Horie-Inoue K, and Inoue S. TRIM47 activates NF-κB signaling via PKC-ε/PKD3 stabilization and contributes to endocrine therapy resistance in breast cancer. *Proceedings of the National Academy of Sciences of the United States of America.* 2021;118(35).
28. Chi W, Wu E, and Morgan BA. Dermal papilla cell number specifies hair size, shape and cycling and its reduction causes follicular decline. *Development (Cambridge, England).* 2013;140(8):1676-83.
29. Hsu YC, Pasolli HA, and Fuchs E. Dynamics between stem cells, niche, and progeny in the hair follicle. *Cell.* 2011;144(1):92-105.
30. Purba TS, Haslam IS, Poblet E, Jiménez F, Gandarillas A, Izeta A, et al. Human epithelial hair follicle stem cells and their progeny: current state of knowledge, the widening gap in translational research and future challenges. *BioEssays : news and reviews in molecular, cellular and developmental biology.* 2014;36(5):513-25.
31. Bray SJ. Notch signalling in context. *Nature reviews Molecular cell biology.* 2016;17(11):722-35.
32. Shimomura Y, Agalliu D, Vonica A, Luria V, Wajid M, Baumer A, et al. APCDD1 is a novel Wnt inhibitor mutated in hereditary hypotrichosis simplex. *Nature.* 2010;464(7291):1043-7.
33. Levy-Nissenbaum E, Betz RC, Frydman M, Simon M, Lahat H, Bakhan T, et al. Hypotrichosis simplex of the scalp is associated with nonsense mutations in CDSN encoding corneodesmosin. *Nature genetics.* 2003;34(2):151-3.
34. Zhang X, Guo BR, Cai LQ, Jiang T, Sun LD, Cui Y, et al. Exome sequencing identified a missense mutation of EPS8L3 in Marie Unna hereditary hypotrichosis. *Journal of medical genetics.* 2012;49(12):727-30.
35. Zhou C, Zang D, Jin Y, Wu H, Liu Z, Du J, et al. Mutation in ribosomal protein L21 underlies hereditary hypotrichosis simplex. *Human mutation.* 2011;32(7):710-4.
36. Pasternack SM, Refke M, Paknia E, Hennies HC, Franz T, Schäfer N, et al. Mutations in SNRPE, which encodes a core protein of the spliceosome, cause autosomal-dominant hypotrichosis simplex. *American journal of human genetics.* 2013;92(1):81-7.
37. Yu X, Chen F, Ni C, Zhang G, Zheng L, Zhang J, et al. A Missense Mutation

within the Helix Termination Motif of KRT25 Causes Autosomal Dominant Woolly Hair/Hypotrichosis. *The Journal of investigative dermatology.* 2018;138(1):230-3.
38. Li M, Cheng R, Zhuang Y, and Yao Z. A recurrent mutation in the APCDD1 gene responsible for hereditary hypotrichosis simplex in a large Chinese family. *The British journal of dermatology.* 2012;167(4):952-4.
39. Shimomura Y. Congenital hair loss disorders: rare, but not too rare. *The Journal of dermatology.* 2012;39(1):3-10.
40. Peters LL, Robledo RF, Bult CJ, Churchill GA, Paigen BJ, and Svenson KL. The mouse as a model for human biology: a resource guide for complex trait analysis. *Nature reviews Genetics.* 2007;8(1):58-69.
41. Searle AG, Edwards JH, and Hall JG. Mouse homologues of human hereditary disease. *Journal of medical genetics.* 1994;31(1):1-19.
42. Kuehn MR, Bradley A, Robertson EJ, and Evans MJ. A potential animal model for Lesch-Nyhan syndrome through introduction of HPRT mutations into mice. *Nature.* 1987;326(6110):295-8.
43. Guibinga GH, Hsu S, and Friedmann T. Deficiency of the housekeeping gene hypoxanthine-guanine phosphoribosyltransferase (HPRT) dysregulates neurogenesis. *Molecular therapy : the journal of the American Society of Gene Therapy.* 2010;18(1):54-62.
44. Pavlenko E, Cabron AS, Arnold P, Dobert JP, Rose-John S, and Zunke F. Functional Characterization of Colon Cancer-Associated Mutations in ADAM17: Modifications in the Pro-Domain Interfere with Trafficking and Maturation. *International journal of molecular sciences.* 2019;20(9).
45. Blaydon DC, Biancheri P, Di WL, Plagnol V, Cabral RM, Brooke MA, et al. Inflammatory skin and bowel disease linked to ADAM17 deletion. *The New England journal of medicine.* 2011;365(16):1502-8.
46. Imoto I, Saito M, Suga K, Kohmoto T, Otsu M, Horiuchi K, et al. Functionally confirmed compound heterozygous ADAM17 missense loss-of-function variants cause neonatal inflammatory skin and bowel disease 1. *Scientific reports.* 2021;11(1):9552.
47. Hatakeyama S. TRIM Family Proteins: Roles in Autophagy, Immunity, and Carcinogenesis. *Trends in biochemical sciences.* 2017;42(4):297-311.
48. Kubo S, Fritz JM, Raquer-McKay HM, Kataria R, Vujkovic-Cvijin I, Al-Shaibi A, et al. Congenital iRHOM2 deficiency causes ADAM17 dysfunction and environmentally directed immunodysregulatory disease. *Nature immunology.* 2022;23(1):75-85.
49. Li X, Maretzky T, Weskamp G, Monette S, Qing X, Issuree PD, et al. iRhoms 1 and 2 are essential upstream regulators of ADAM17-dependent EGFR signaling. *Proceedings of the National Academy of Sciences of the United States of America.* 2015;112(19):6080-5.
50. Adu-Amankwaah J, Adzika GK, Adekunle AO, Ndzie Noah ML, Mprah R, Bushi A, et al. ADAM17, A Key Player of Cardiac Inflammation and Fibrosis in Heart Failure Development During Chronic Catecholamine Stress. *Frontiers*

in cell and developmental biology. 2021;9:732952.
51. Xu P, and Derynck R. Direct activation of TACE-mediated ectodomain shedding by p38 MAP kinase regulates EGF receptor-dependent cell proliferation. *Molecular cell.* 2010;37(4):551-66.
52. Liu G, Cheng G, Zhang Y, Gao S, Sun H, Bai L, et al. Pyridoxine regulates hair follicle development via the PI3K/Akt, Wnt and Notch signalling pathways in rex rabbits. *Animal nutrition (Zhongguo xu mu shou yi xue hui).* 2021;7(4):1162-72.
53. Sakamoto K, Jin SP, Goel S, Jo JH, Voisin B, Kim D, et al. Disruption of the endopeptidase ADAM10-Notch signaling axis leads to skin dysbiosis and innate lymphoid cell-mediated hair follicle destruction. *Immunity.* 2021;54(10):2321-37.e10.
54. Vauclair S, Nicolas M, Barrandon Y, and Radtke F. Notch1 is essential for postnatal hair follicle development and homeostasis. *Developmental biology.* 2005;284(1):184-93.
55. Revandkar A, Perciato ML, Toso A, Alajati A, Chen J, Gerber H, et al. Inhibition of Notch pathway arrests PTEN-deficient advanced prostate cancer by triggering p27-driven cellular senescence. *Nature communications.* 2016;7:13719.
56. Baumgart A, Seidl S, Vlachou P, Michel L, Mitova N, Schatz N, et al. ADAM17 regulates epidermal growth factor receptor expression through the activation of Notch1 in non-small cell lung cancer. *Cancer research.* 2010;70(13):5368-78.
57. Wang R, Li Y, Tsung A, Huang H, Du Q, Yang M, et al. iNOS promotes CD24(+)CD133(+) liver cancer stem cell phenotype through a TACE/ADAM17-dependent Notch signaling pathway. *Proceedings of the National Academy of Sciences of the United States of America.* 2018;115(43):E10127-e36.
58. Weber S, Niessen MT, Prox J, Lüllmann-Rauch R, Schmitz A, Schwanbeck R, et al. The disintegrin/metalloproteinase Adam10 is essential for epidermal integrity and Notch-mediated signaling. *Development (Cambridge, England).* 2011;138(3):495-505.
59. Pan D, and Rubin GM. Kuzbanian controls proteolytic processing of Notch and mediates lateral inhibition during Drosophila and vertebrate neurogenesis. *Cell.* 1997;90(2):271-80.
60. Sotillos S, Roch F, and Campuzano S. The metalloprotease-disintegrin Kuzbanian participates in Notch activation during growth and patterning of Drosophila imaginal discs. *Development (Cambridge, England).* 1997;124(23):4769-79.
61. Rooke J, Pan D, Xu T, and Rubin GM. KUZ, a conserved metalloprotease-disintegrin protein with two roles in Drosophila neurogenesis. *Science (New York, NY).* 1996;273(5279):1227-31.
62. Alabi RO, Lora J, Celen AB, Maretzky T, and Blobel CP. Analysis of the Conditions That Affect the Selective Processing of Endogenous Notch1 by ADAM10 and ADAM17. *International journal of molecular sciences.*

2021;22(4).
63. Bozkulak EC, and Weinmaster G. Selective use of ADAM10 and ADAM17 in activation of Notch1 signaling. *Molecular and cellular biology.* 2009;29(21):5679-95.
64. Groot AJ, Cobzaru C, Weber S, Saftig P, Blobel CP, Kopan R, et al. Epidermal ADAM17 is dispensable for notch activation. *The Journal of investigative dermatology.* 2013;133(9):2286-8.
65. Shimizu H, Hosseini-Alghaderi S, Woodcock SA, and Baron M. Alternative mechanisms of Notch activation by partitioning into distinct endosomal domains. *The Journal of cell biology.* 2024;223(5).
66. Brou C, Logeat F, Gupta N, Bessia C, LeBail O, Doedens JR, et al. A novel proteolytic cleavage involved in Notch signaling: the role of the disintegrin-metalloprotease TACE. *Molecular cell.* 2000;5(2):207-16.
67. Dixit G, Gonzalez-Bosquet J, Skurski J, Devor EJ, Dickerson EB, Nothnick WB, et al. FGFR2 mutations promote endometrial cancer progression through dual engagement of EGFR and Notch signalling pathways. *Clinical and translational medicine.* 2023;13(5):e1223.
68. Li M, Cheng R, Liang J, Yan H, Zhang H, Yang L, et al. Mutations in POFUT1, encoding protein O-fucosyltransferase 1, cause generalized Dowling-Degos disease. *American journal of human genetics.* 2013;92(6):895-903.
69. Chen F, Ni C, Wang X, Cheng R, Pan C, Wang Y, et al. S1P defects cause a new entity of cataract, alopecia, oral mucosal disorder, and psoriasis-like syndrome. *EMBO molecular medicine.* 2022;14(5):e14904.

Figure and Figure Legends

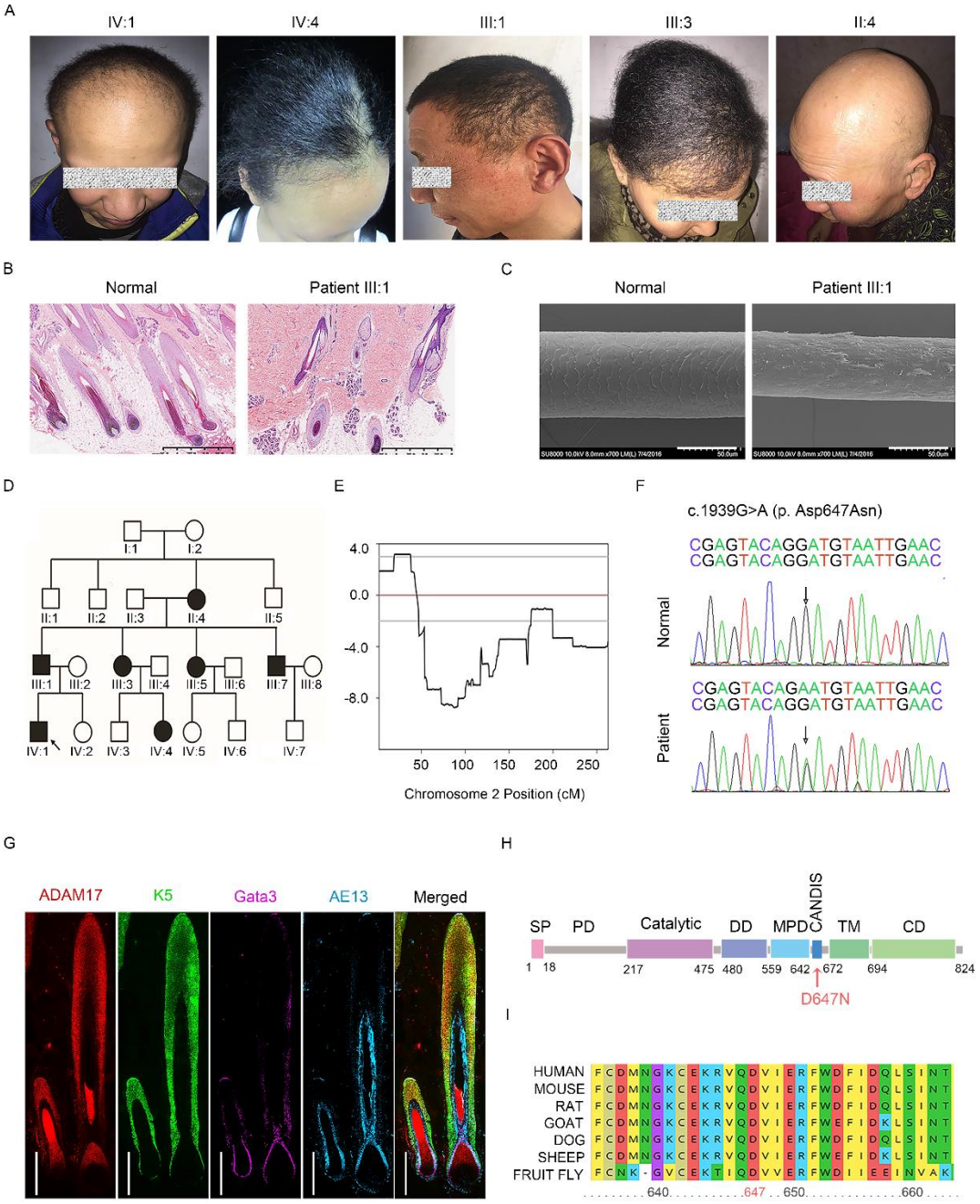

Fig. 1. *ADAM17* variant leads to autosomal dominant hypotrichosis with woolly hair.

(**A**) Representative clinical pictures of patients with autosomal dominant hypotrichosis/woolly hair (ADHW). (**B**) Hematoxylin and eosin (HE) staining of scalp

tissues from patients and the normal controls. Scale bars, 125 μm. (**C**) The scanning electron microscope analysis revealed that the patient's hair shaft displayed a non-uniform and abnormal cross-sectional shape. Furthermore, there was a substantial peeling of hair cuticle, which normally functioned as the hair shaft's outermost protective layer. Scale bars, 50 μm. (**D**) Pedigree of the family for patients. Hollow boxes represented the normal male individuals, while solid boxes represented the affected male patients. Hollow circles represented the normal female individuals, while solid circles represented the affected female patients in the family tree. The proband was identified with a black arrow. (**E**) A genome-wide linkage analysis provided evidence of linkage to chromosome 2, with a maximum LOD score of 3.18. (**F**) Gene sequencing revealed the heterozygous *ADAM17* p. Asp647Asn (c.1939G>A) variant in patients. The arrows indicate the variant. (**G**) ADAM17 was predominantly expressed in the hair cortex, inner root sheath (IRS), and outer root sheath (ORS) of human hair follicle. Scale bar, 500 μm. (**H**) Schematic overview of ADAM17 protein and its domains. SP, signal peptide; PD, pro-domain; Catalytic, catalytic metalloprotease domain; DD, disintegrin domain; MPD, membrane proximal domain; CANDIS, conserved ADAM17 seventeen dynamic interaction sequence; TM, transmembrane domain; CD, cytoplasmic domain. The p.D647N mutation was localized in CANDIS domain (indicated by a red arrow). (**I**) Aspartic residue at position 647 is located within the conserved ADAM17 seventeen dynamic interaction sequence (CANDIS) domain of ADAM17, which is highly conserved.

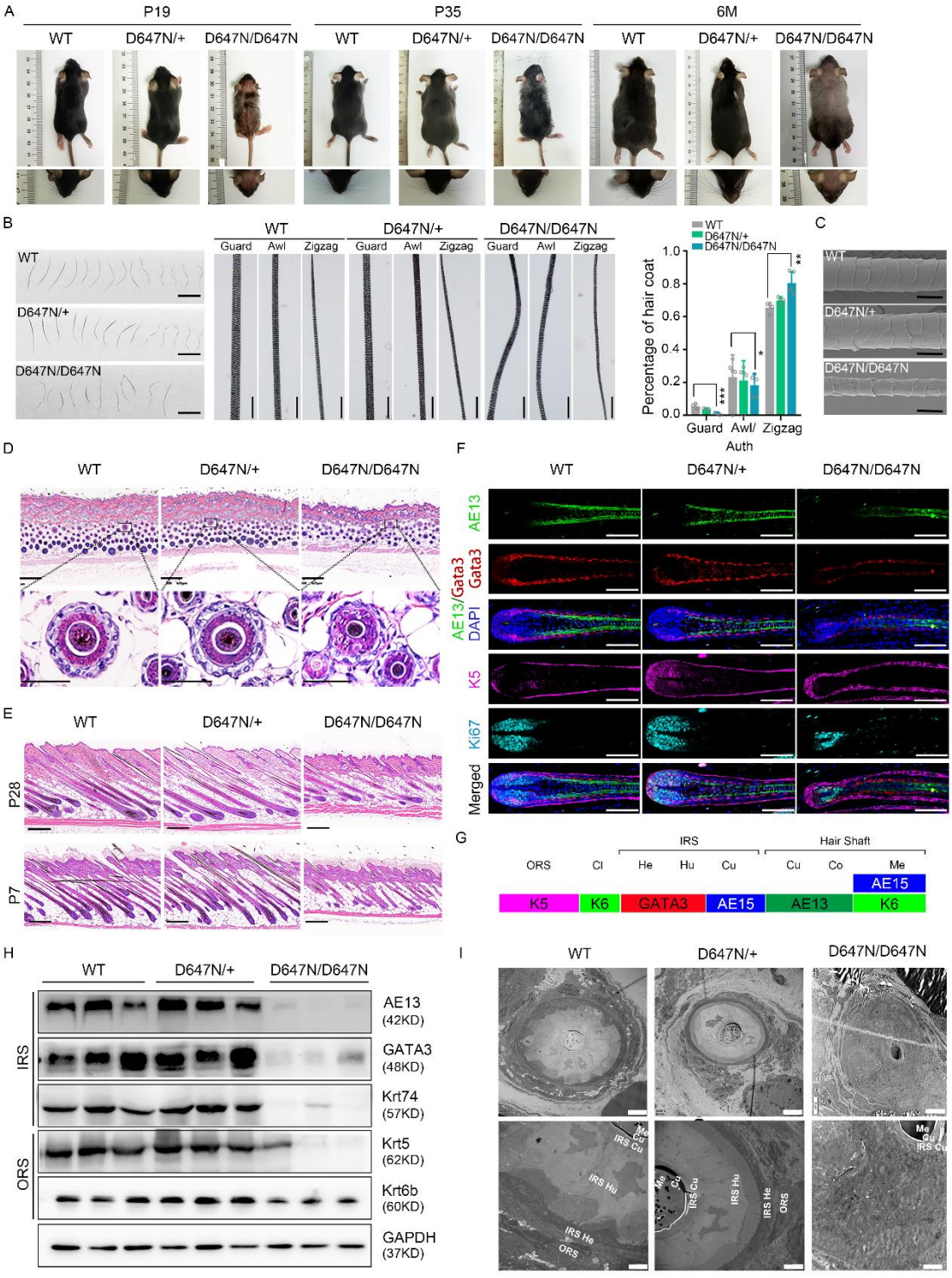

Fig. 2. *Adam17* (p.D647N) variant causes abnormal hair follicle morphology and hair loss in mice.

(A) Hair coats and vibrissa hairs of wild-type (WT), $Adam17^{D647N/+}$ and $Adam17^{D647N/D647N}$ mice at postnatal day (P) 19, P35 and 6 months (M). (**B**) Pelage hairs

were observed under an optical microscope. Left and middle panel: compared with wild-type hairs, all of four hair types of Adam17$^{D647N/D647N}$ pelage hairs showed waviness. Scale bars, 2 mm. Right panel: Adam17$^{D647N/D647N}$ mice displayed a significantly reduced proportion of primary and secondary hairs and a significant increase in the proportion of zigzag hairs. (n = 4 biological replicates). (**C**) The scanning electron microscope analysis unveiled a significant peeling of the hair cuticle in the hair of Adam17$^{D647N/D647N}$ mice. (**D**) HE staining revealed a notable structural abnormalities of hair follicles in Adam17$^{D647N/D647N}$ mice at P28. Upper panel scale bars, 250 μm; lower panel scale bars, 50 μm; (**E**) HE staining of longitudinal sections revealed obvious structural abnormalities of hair follicles in Adam17$^{D647N/D647N}$ mice during the first anagen (P7) and second anagen (P28). Scale bars, 250 μm. (**F**) Immunofluorescence staining revealed a substantial decrease in IRS markers within the hair follicles of Adam17$^{D647N/D647N}$ mice, suggesting significant morphological abnormalities of the IRS. Scale bar, 100 μm. (**G**) A schematic illustration of hair follicle layers and markers expressed in hair follicle. (**H**) Immunoblot analysis of hair follicle layer-specific markers in dorsal skin. (**I**) Transmission electron microscopy of hair follicles at approximately 500 μm depth. Left panel scale bar, 5 μm; Right panel scale bar, 2 μm. ORS, outer root sheath; IRS, inner root sheath; Cl, companion layer; He, Henle's layer; Hu, Huxley's layer; Cu, cuticle; Co, cortex; Me, medulla. All experiments were repeated three times. Results were expressed as mean ± SD; n.s., not significant; *$P < 0.05$; **$P < 0.01$; ***$P < 0.001$; One-way ANOVA (B).

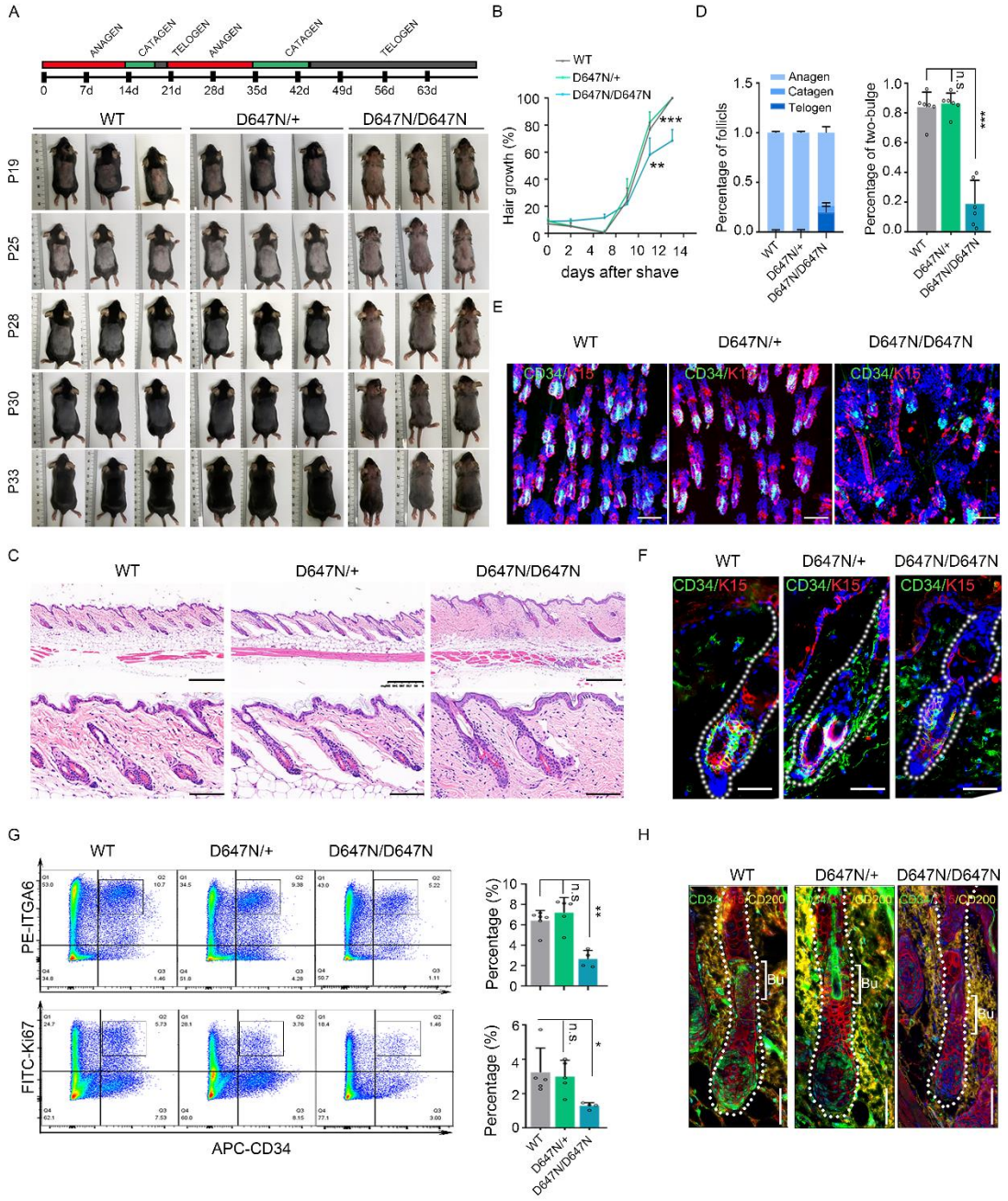

Fig. 3. *Adam17* (p.D647N) variant affects homeostasis of the hair follicle stem cell (HFSCs) niche in hair follicles.

(**A**) Phenotypes of wild-type, Adam17$^{D647N/+}$ and Adam17$^{D647N/D647N}$ mice after shaving back skins during telogen (P19), monitoring initiation of the next hair cycle. *Adam17* (p.D647N) mutation impeded hair regeneration. (**B**) Statistical data on the proportion of the skin with pigmentation in mice after hair shaving. (n = 6 biological replicates).

(**C**) HE staining of back skins during second telogen (P63). Upper panel scale bars, 300 μm; lower panel scale bars, 50 μm. (**D**-**F**) Wild-type hair follicles (HFs) possessed a two-bulge architecture, whereas Adam17$^{D647N/D647N}$ HFs usually had only one. (**D**) Statistical data on the proportion of three hair follicle types. (n = 6 biological replicates). (**E**) Immunofluorescence was performed on whole-mount back skin hair follicles at the second telogen stage using HFSCs markers K15 and CD34. Scale bar, 100 μm. (**F**) Skin sections underwent immunofluorescent staining using antibodies specific to HFSCs markers. Scale bars, 40 μm. (**G**) Fluorescence activated cell sorting (FACS) analyses of HFSCs populations sorted by high 6-integrin and CD34. Right upper panel: Quantification of CD34 positive/α6 high cells (indicated by the black square brackets) among epithelial cells in second telogen mice. (n = 4-6 biological replicates). Right lower panel: Quantification of CD34 positive/Ki67positive cells among epithelial cells in second telogen mice. (n = 4-6 biological replicates). (**H**) HFSCs differentiation was blocked in Adam17$^{D647N/D647N}$ mice. CD200, the marker of secondary hair germ. Scale bars, 40 μm. All experiments were repeated three times. Results were expressed as mean ± SD; n.s., not significant; *P < 0.05; **P < 0.01; ***P < 0.001; One-way ANOVA (B, D); Mann-Whitney test (G: Right upper panel); Kruskal-Wallis test (G: Right lower panel).

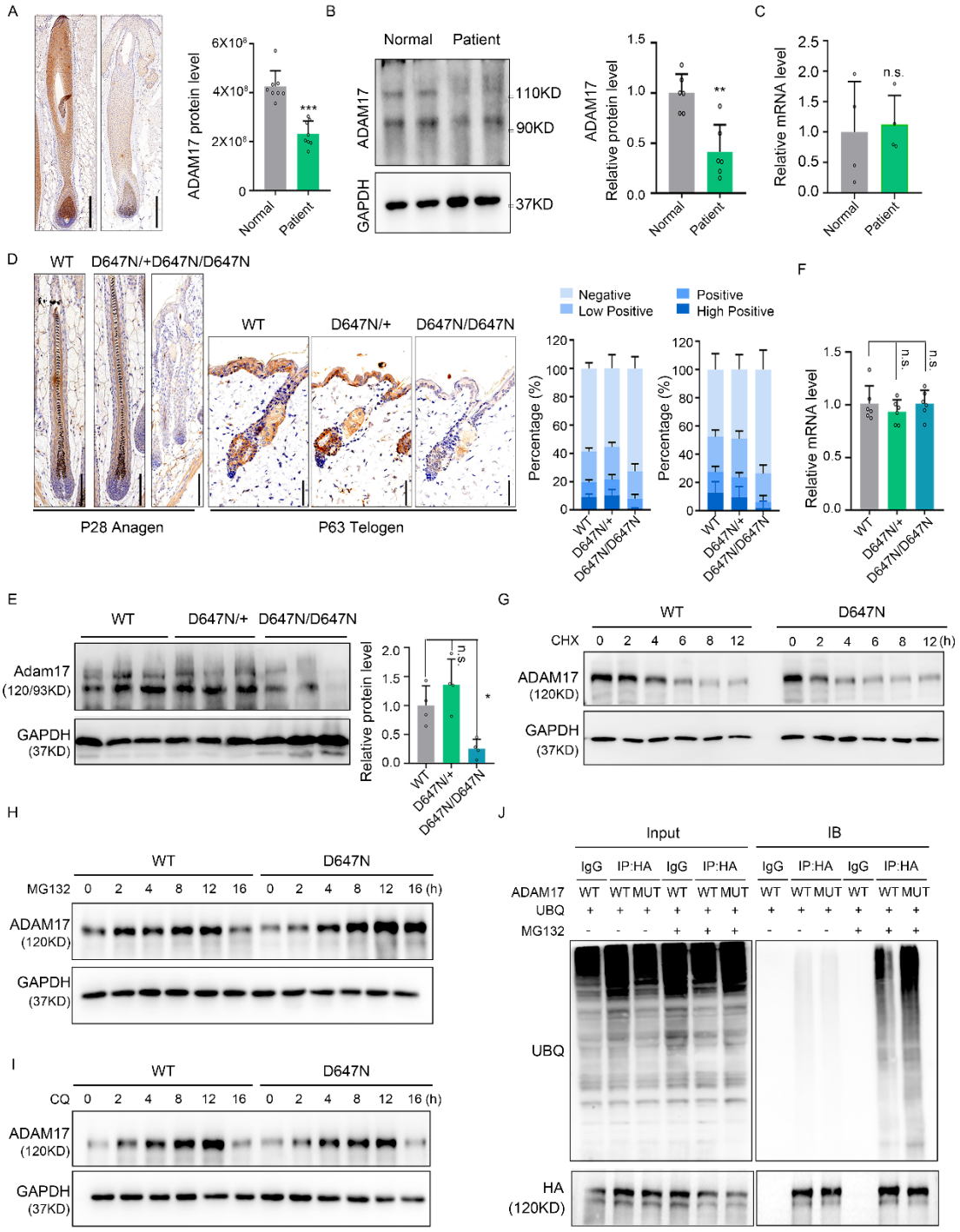

Fig. 4. *ADAM17* (p.D647N) variant decreases its protein stability owing to enhanced auto-ubiquitination.

(**A**) Immunohistochemical staining showed that the expression of ADAM17 in patients' hair follicles was significantly lower than that in normal controls. Scale bar, 300 μm;

(n = 8 biological replicates of normal controls; n = 8 technical replicates of patient III:1). (**B**) ADAM17 protein level in the scalp tissues of patients was lower than that in the normal controls. (n = 6 biological replicates of normal controls; n = 6 technical replicates of patient III:1). (**C**) No significant alteration detected in the mRNA levels of *ADAM17*. (n = 4 biological replicates of normal controls; n = 4 technical replicates of patient III:1). (**D**) Adam17 protein level in hair follicles of $Adam17^{D647N/D674N}$ mice was significantly lower than that in wild-type mice. Left scale bar, 100 μm. Right scale bar, 50 μm. (n = 28-32 technical replicates). (**E**) Adam17 protein level in skin tissues was significantly reduced in $Adam17^{D647N/D674N}$ mice compared to the wild-type mice. (n = 3 biological replicates). (**F**) No significant changes were observed in the mRNA levels of *Adam17* between $ADAM17^{D647N/D674N}$ and wild-type mice. (n = 6 biological replicates). (**G**) Cycloheximide (CHX) chase analysis showed that *ADAM17* (p.D674N) mutation induced rapid degradation of ADAM17 in HaCaT cells. (**H**) *ADAM17* (p.D647N) mutation resulted in heightened degradation of ADAM17 though proteasome pathway in HaCaT cells. (**I**) *ADAM17* (p.D647N) mutation had no bearing on the degradation of ADAM17 through the autophagy pathway in HaCaT cells. (**J**) *ADAM17* (p.D647N) mutation resulted in heightened ubiquitination and subsequent degradation of ADAM17 via the proteasomal pathway. All experiments were repeated three times. Results were expressed as mean ± SD; n.s., not significant; **P* < 0.05; ***P* < 0.01; ****P* < 0.001; Unpaired two-tailed t test (B, C); One-way ANOVA (E, F); Mann-Whitney test (A).

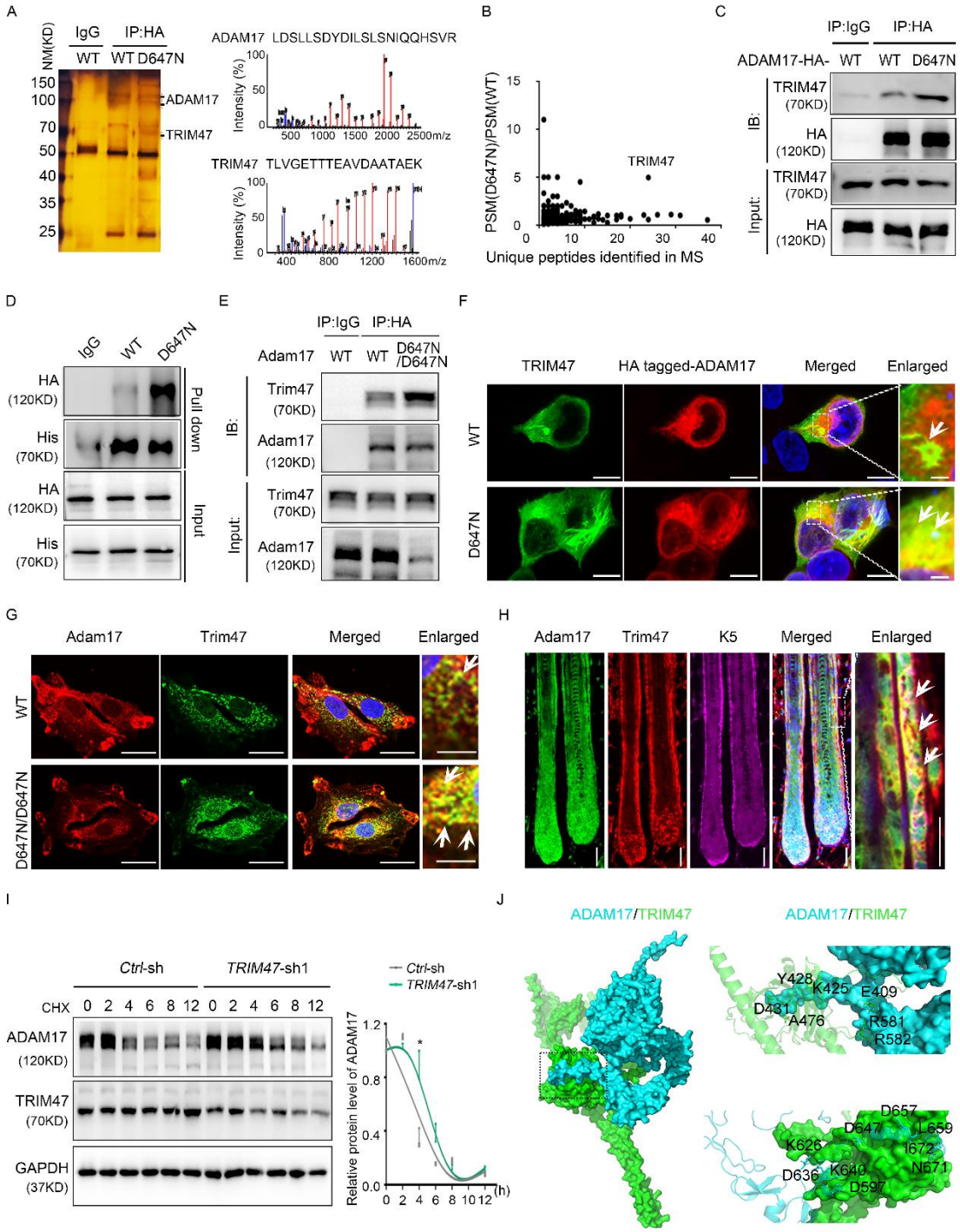

Fig. 5. TRIM47 is identified as a specific E3 ubiquitin ligase of ADAM17.

(A) LC-MS/MS analysis of wild-type and mutant ADAM17 binding proteins. (B) PSM (peptide spectrum match) score ratios for the proteins identified by mass spectrometry.

928 (**C**) Co-immunoprecipitation assays indicated that ADAM17 interacts with TRIM47 in
929 HaCaT cells, and their association was enhanced by the *ADAM17* (p.D647N) mutation.
930 HaCaT cells lysates were collected and subjected to co-immunoprecipitation assay
931 using indicated antibodies. (**D**) The direct interaction between ADAM17 and TRIM47
932 was validated by pull-down assay. *In vitro*–translated ADAM17 was pulled down by
933 purified His tagged-TRIM47 fusion protein. (**E**) Endogenous association between
934 Adam17 and Trim47 was verified in the epidermal tissue lysates of mice, and *Adam17*
935 (p.D647N) mutation enhanced their association. (**F**) Confocal immunofluorescence
936 revealed a co-localization (yellow) of ADAM17 (red) and TRIM47 (green) in HaCaT
937 cells, and *ADAM17* (p.D647N) mutation enhanced their co-localization. Scale bars, 8
938 μm (panels 1-3); scale bars, 1 μm (panel 4). (**G**) Confocal immunofluorescence revealed
939 a co-localization (yellow) of Adam17 (red) and Trim47 (green) in primary cultured
940 mouse skin fibroblasts. Scale bars, 10 μm (panels 1-3); scale bars, 1 μm (panel 4). (**H**)
941 Adam17 and Trim47 co-localized in both IRS and ORS of hair follicles. The white
942 arrows indicated the co-localization (yellow) of Trim47 (green) and Adam17 (red).
943 Scale bars, 40 μm (panels 1- 4); Scale bars, 20 μm (panel 5). (**I**) Knockdown of *TRIM47*
944 impeded the proteasomal degradation of ADAM17. Left panel: Representative
945 immunoblot images of the ADAM17 and TRIM47 protein levels during CHX chase
946 assays. Right panel: quantification of immunoblotting results corresponding to the left
947 panel. (n = 3 biological replicates). (**J**) The three-dimensional structure of
948 ADAM17/TRIM47 complex in stereo. Right upper panel: essential amino acids of
949 ADAM17 (blue) which polar contacted to TRIM47 (green) were depicted in atom-

colored stick. Right lower panel: residues of TRIM47 (green) which polar contacted to ADAM17 (blue) were depicted in atom-colored stick. All experiments were repeated three times. Results were expressed as mean ± SD; ns, not significant; *$P < 0.05$; Unpaired two-tailed t test (G).

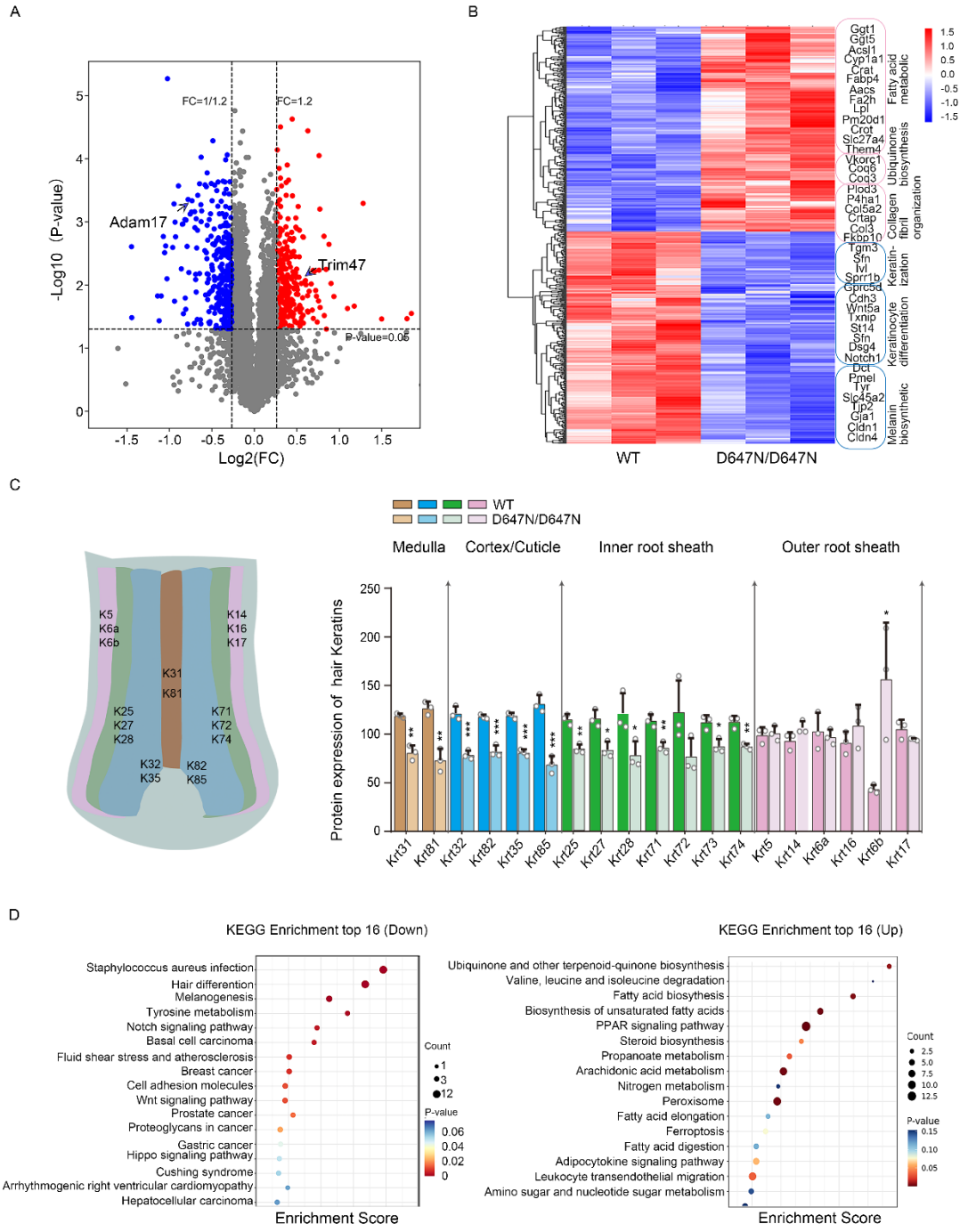

Fig.6. ADAM17 variant inhibits hair follicle development through the Notch signaling pathway.

(**A**) Log2-fold change in the normalized counts of Proteomics-seq reads of differentially expressed proteins (DEPs) in wild-type and Adam17$^{D647N/D647N}$ mice. (**B**) Heatmap of

DEPs in the indicated mice, annotated for selected proteins. (**C**) DEPs analysis revealed a substantial decrease of hair shaft and IRS markers in Adam17$^{D647N/D647N}$ mice. (n = 3 biological replicates). (**D**) Pathway enrichment analysis of DEPs revealed marked up-regulation of ubiquinone and other terpenoid-quinone biosynthesis pathways and down-regulation of Notch signaling pathways. Results were expressed as mean ± SD; **P* < 0.05; ***P* < 0.01; ****P* < 0.001; Unpaired two-tailed t test (**C**).

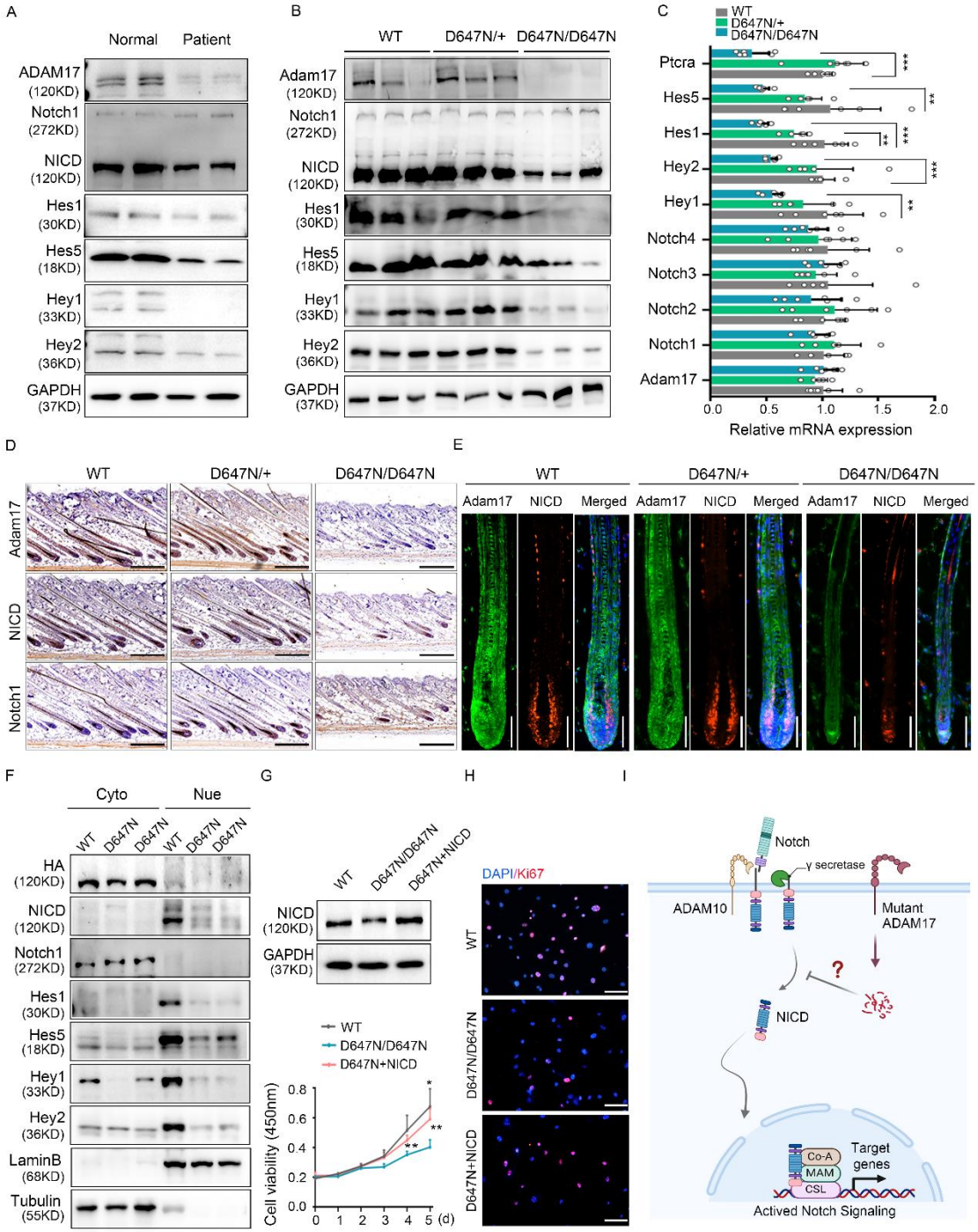

Fig.7. *ADAM17* (p.D647N) variant affects Notch signaling resulting in HFs malformation.

(**A**) Effects of *ADAM17* (p.D647N) mutation on protein levels of key molecules involved in Notch signaling observed in the skin biopsy of the patient. (**B**) *Adam17*

(p.D647N) mutation inhibited Notch signaling in the skin tissues of mice. (**C**) Effects of *Adam17* (p.D647N) mutation on mRNA levels of key molecules involved in Notch signaling observed in the skin tissues of mice. (n = 6 biological replicates). (**D**) Immunohistochemical staining showed that *Adam17* (p.D647N) mutation led to down-regulation of ADAM17 and Notch intracellular domain (NICD) expression, but not full-length Notch1 in Adam17$^{D647N/D647N}$ mice. Scale bar, 250 μm. (**E**) Immunofluorescence showed that *Adam17* (p.D647N) mutation led to down-regulation of Adam17 and Notch intracellular domain (NICD) expression in hair follicle of Adam17$^{D647N/D647N}$ mice. Scale bar, 80 μm. (**F**) Cellular component separation assay showed that NICD protein level was decreased in nucleus of ADAM17 mutant HaCaT cells. LaminB2 and a-Tubulin were used as the nuclear, cytosolic protein makers, respectively. (**G-H**) Overexpressing NICD significantly rescued the proliferation activity of primary fibroblasts derived from Adam17$^{D647N/D647N}$ mice. (n = 3 biological replicates). (**I**) Schematic diagram of Notch signaling pathway. Following sequentially cleaved by ADAM10 and γ-secretase, Notch released its intracellular domain (NICD). NICD then translocated to nucleus, and in collaboration with RBPJ and Mastermind, activated the transcription of target genes including members of the *Hes* and *Hey* families. All experiments were repeated three times. Results were expressed as mean ± SD; **P* < 0.05; ***P* < 0.01; ****P* < 0.001; One-way ANOVA and Kruskal-Wallis test (C); Brown-Forsythe and Welch ANOVA tests (G).